Biochimica et Biophysica Acta 1837 (2014) 920–928

Contents lists available at ScienceDirect

Biochimica et Biophysica Acta

journal homepage: www.elsevier.com/locate/bbabio

Thermodynamic and kinetic characterization of two methyl-accepting chemotaxis heme sensors from *Geobacter sulfurreducens* reveals the structural origin of their functional difference

Marta A. Silva [a], Raquel C. Valente [a], P. Raj Pokkuluri [b], David L. Turner [c], Carlos A. Salgueiro [a,*], Teresa Catarino [c,d,**]

[a] Requimte-CQFB, Departamento de Química, Faculdade de Ciências e Tecnologia, Universidade Nova de Lisboa, Campus Caparica, 2829-516 Caparica, Portugal
[b] Biosciences Division, Argonne National Laboratory, Lemont, IL 60439, USA
[c] Instituto de Tecnologia Química e Biológica, Universidade Nova de Lisboa, Av. da República, 2780-157 Oeiras, Portugal
[d] Departamento de Química, Faculdade de Ciências e Tecnologia, FCT, Universidade Nova de Lisboa, 2829-516 Caparica, Portugal

ARTICLE INFO

Article history:
Received 10 December 2013
Received in revised form 8 January 2014
Accepted 13 January 2014
Available online 24 January 2014

Keywords:
c-Type heme sensor
Geobacter
Redox potential
Signal transduction
Electron transfer kinetics

ABSTRACT

The periplasmic sensor domains GSU582 and GSU935 are part of methyl-accepting chemotaxis proteins of the bacterium *Geobacter sulfurreducens* containing one *c*-type heme and a PAS-like fold. Their spectroscopic properties were shown previously to share similar spectral features. In both sensors, the heme group is in the high-spin form in the oxidized state and low-spin after reduction and binding of a methionine residue. Therefore, it was proposed that this redox-linked ligand switch might be related to the signal transduction mechanism. We now report the thermodynamic and kinetic characterization of the sensors GSU582 and GSU935 by visible spectroscopy and stopped-flow techniques, at several pH and ionic strength values. Despite their similar spectroscopic features, the midpoint reduction potentials and the rate constants for reduction by dithionite are considerably different in the two sensors. The reduction potentials of both sensors are negative and well framed within the typical anoxic subsurface environments in which *Geobacter* species predominate. The midpoint reduction potentials of sensor GSU935 are lower than those of GSU582 at all pH and ionic strength values and the same was observed for the reduction rate constants. The origin of the different functional properties of these closely related sensors is rationalized in the terms of the structures. The results suggest that the sensors are designed to function in different working potential ranges, allowing the bacteria to trigger an adequate cellular response in different anoxic subsurface environments. These findings provide an explanation for the co-existence of two similar methyl-accepting chemotaxis proteins in *G. sulfurreducens*.

© 2014 Elsevier B.V. All rights reserved.

1. Introduction

The bacterial environment is constantly changing due to variations in physicochemical parameters such as temperature, nutritional opportunities, environmental gases, light, or oxygen tension. Signal transduction systems establish intracellular information-processing networks that link external stimuli to specific adaptive responses [1–3]. Bacterial heme-based sensors constitute an important group of proteins that exploit the redox chemistry of the heme group to sense environmental changes [4–10]. The more common heme-based sensors contain a *b*-type heme in the sensor domain that could bind effector molecules such as O_2, NO, or CO [11,12]. These proteins typically comprise a regulatory heme-binding domain (sensor domain) coupled to a neighboring transmitter (transduction domain). In functional terms, the binding of a physiological effector to the heme triggers the signal transduction process by conformational changes at the transduction domain, which generates the intracellular signal and concomitant regulation of the physiological response [4–10]. The residues located in the neighborhood of the heme play a crucial role in discriminating the physiological ligand from other possible ligands since the intramolecular signal transduction cascade is initiated by local conformational changes in this region. Therefore, discrimination and selection of the correct stimulus is crucial for triggering an adequate appropriate response. This is a particular challenge for the *Geobacter* bacteria whose remarkable respiratory versatility allows the microorganisms to proliferate in quite distinct environments [for a review see [13]]. The versatility showed by the bacterium *Geobacter sulfurreducens* (*Gs*) might explain the coexistence of a large number of heme-based sensors since an efficient metabolic switch is necessary to respond to the exhaustion of a particular electron acceptor, the appearance of a different electron donor, or even a change in the

* Correspondence to: C.A. Salgueiro, Departamento Química, Faculdade de Ciências e Tecnologia, Universidade Nova de Lisboa, Campus Caparica, 2829-516 Caparica, Portugal. Tel.: +351 212 948 300; fax: +351 212 948 385.
** Correspondence to: T. Catarino, Instituto de Tecnologia Química e Biológica, Universidade Nova de Lisboa, Av. da República, 2780-157 Oeiras, Portugal. Tel.: +351 214 469 718; fax: +351 214 411 277.
E-mail addresses: csalgueiro@fct.unl.pt (C.A. Salgueiro), catarino@itqb.unl.pt (T. Catarino).

0005-2728/$ – see front matter © 2014 Elsevier B.V. All rights reserved.
http://dx.doi.org/10.1016/j.bbabio.2014.01.008

redox potential of the environment. Indeed, ten periplasmic sensor domains were found in *Gs* genome, each containing at least one heme *c*-binding motif [14]. Another heme containing sensor, DcrA from *Desulfovibrio vulgaris* [15,16] was also reported. The *Gs* periplasmic heme sensor domains are part of proteins described as two-component signal transduction or chemotaxis proteins and have homologs in other *Geobacter* species [17]. The *Gs* heme sensors, encoded by genes *gsu0582* and *gsu0935* (hereafter designated GSU582 and GSU935), are parts of methyl-accepting chemotaxis proteins with similar predicted topologies: an N-terminal tail in the cytoplasm, followed by a transmembrane helix, a periplasmic domain (about 135 residues), another transmembrane helix, and cytoplasmic domains consisting of a HAMP domain followed by a methyl-accepting chemotaxis protein domain [for a review see [17,18]]. The sensor domains of GSU582 and GSU935 have been structurally and biochemically characterized and, despite their moderate sequence homology (see Figure S1 in Supplementary Material), they show remarkably similar spectroscopic features, as revealed by UV–visible, EPR, NMR and RR spectroscopies [11,17]: (i) the heme group is high-spin in the oxidized state and becomes low-spin after reduction upon binding of a methionine (probably Met60) at the heme distal site; (ii) both sensors bind carbon monoxide (CO) in the reduced form and nitric oxide (NO) in the reduced and oxidized forms; (iii) binding of CO or NO to the reduced proteins occurs by replacing the axial ligand Met60; and (iv) the binding/dissociation of CO or NO is fully reversible. More recently, CO and NO binding studies showed that ferrous GSU582 and GSU935 sensors have high and similar affinity towards these molecules but, in the ferric form, sensor GSU582 shows a much higher affinity for NO [11].

The structures of both sensor domains have been determined and showed that they have a PAS-like fold and form swapped dimers [17]. Therefore, it was suggested that sensors GSU935 and GSU582 might trigger the signal transduction mechanism in a process that involves the formation of the swapped dimer in the periplasm with the concomitant alteration of the relative positions of the transmembrane helices and response of the cytoplasmic transducer domains. Collecting all the available information for these sensor domains, it was proposed that the change of the redox state coupled to heme spin state/coordination alteration could initiate the signal transduction mechanism [11]. In such a mechanism, the protein is kept blocked in the inactive/ferrous state, until a change in the environment redox potential oxidizes the protein, releases Met60 and allows activation. This hypothesis, reinforced by the significant differences observed in the low reduction potential values of GSU582 and GSU935 sensors previously obtained at pH 8 [17], suggests that the proteins could work as redox sensors for chemotaxis. To further understand the functional differences between the two sensors, we performed a detailed thermodynamic and kinetic characterization of their redox behavior within the physiological pH range and rationalized the results in terms of the sequence and structural determinants.

2. Materials and methods

2.1. Expression and purification

The heme-containing sensor domains of GSU582 and GSU935 were expressed and purified as previously described [17]. Briefly, *Escherichia coli* SF110 cells containing the plasmid pEC86 that encodes for the cytochrome *c* maturation gene cluster [19] were transformed with the sensor plasmids, which were cloned as C-terminal fusions to elastin-like polypeptide (ELP) tag and a cleavage site for TEV protease. Cells were grown aerobically at 30 °C in 2xYT medium to mid-exponential phase and after reaching an OD_{600} of ~1.5 were induced with 30 μM isopropyl β-D-thiogalactoside (IPTG). After an overnight incubation under the same conditions the cells were harvested and the periplasmic fraction was isolated by osmotic shock. A solution of 5 M NaCl was used to trigger ELP precipitation. After this step, the fusion protein was dissolved in 50 mM Tris–HCl (pH 8), 0.5 mM EDTA and incubated with TEV protease. The soluble sensor domains were concentrated, and the buffer was exchanged to 100 mM sodium phosphate buffer (pH 8) in an ultrafiltration cell with a 10 kDa cut-off membrane before loading into a Superdex 75 16/70 gel filtration column (GE Healthcare). The purity of the proteins was confirmed by sodium dodecyl sulfate polyacrylamide gel electrophoresis (SDS-PAGE) stained with Coomassie Blue.

2.2. Redox titrations followed by visible spectroscopy

Anaerobic redox titrations followed by visible spectroscopy were performed inside a glove box (MBraun LABstar) under an argon atmosphere with O_2 levels kept below 0.2 ppm as previously described [17]. The UV–visible spectra were recorded with a Thermo Scientific Evolution™ 300 UV–visible spectrophotometer and the temperature was maintained by using an external circulating bath [20]. The solution potentials were measured using a combined Pt/Ag/AgCl electrode (Crison), calibrated before each titration with freshly prepared saturated solutions of quinhydrone at pH 7 and 4 and checked at the end for stability. The reported values are relative to the standard hydrogen electrode (SHE). Experiments were performed at pH 6, 7 and 8 using 5 mM sodium phosphate buffer at two different ionic strengths (10 mM and 200 mM) and 9 μM protein solutions. To ensure a good equilibrium between the redox centers and the working electrode, a mixture of redox mediators methylene blue (E'_{m7} = 11 mV), gallocyanine (E'_{m7} = 21 mV), indigo tetrasulfonate (E'_{m7} = −30 mV), indigo trisulfonate (E'_{m7} = −70 mV), indigo disulfonate (E'_{m7} = −110 mV), anthraquinone-2,6-disulfonate (E'_{m7} = −185 mV), 2-hydroxy-1,4-naphthoquinone (E'_{m7} = −152 mV), anthraquinone-2-sulfonate (E'_{m7} = −225 mV), safranine O (E'_{m7} = −280 mV), diquat (E'_{m7} = −350 mV), benzyl viologen (E'_{m7} = −345 mV), neutral red (E'_{m7} = −325 mV), and methyl viologen (E'_{m7} = −440 mV) was added to the protein solution. The final concentration of mediators was 2 μM to avoid interference caused by specific binding of mediators to the protein. Each titration consisted of a stepwise reduction using a solution of sodium dithionite, followed by oxidation using a solution of ferricyanide. After each addition of titrant, ample time was allowed for a stable measurement of redox potential to be reached, and a spectrum of the sample was taken in the range 700–400 nm. In order to confirm that the pH is stable, the pH was also measured at the end of each redox titration. The redox titrations were repeated at least twice for each pH value, each time both in the oxidative and reductive directions to check for hysteresis. Reproducibility between the runs was typically better than 5 mV.

2.3. Analysis of thermodynamic data

The reduced fraction of each sensor was determined using the region of the UV–visible spectra containing the α and β bands. The optical influence of the mediators was subtracted by measuring their contribution in this spectral region relative to the straight line connecting the two isosbestic points (509 nm and 565 nm for GSU582; 506 nm and 562 nm for GSU935) flanking the α and β bands according to the method described in the literature [21,22]. The reduction potentials were obtained by fitting the experimental variation of the total reduced fraction to one-electron Nernst equation as previously described [23]. Values of the reduction potentials extrapolated to infinite ionic strength were calculated as described by Quintas et al. [24] (included as Supplementary Material).

2.4. Kinetic experiments

The rate of reduction of GSU582 and GSU935 by sodium dithionite was studied as a function of ionic strength in the pH range 6 to 8. Rapid mixing kinetic experiments were carried out on a HI-TECH Scientific SF-61 DX2 stopped-flow instrument inside an anaerobic chamber

(Mbraun MB 150 I) where the oxygen level was kept below 2 ppm. The temperature was kept at 293 ± 1 K using an external circulating bath. The data were acquired at 401, 414 and 551 nm using a large excess of sodium dithionite to guarantee pseudo-first order kinetics, irreversible electron transfer steps, and the complete reduction of the sensors [24]. At least three data sets for each experimental condition were averaged to increase the signal to noise ratio.

Buffers at different ionic strengths covering the range 10 to 200 mM were prepared by diluting a concentrated NaCl solution in 5 mM sodium phosphate buffer pH 6, 7 and 8 with degassed water inside an anaerobic chamber. Small pH variations were corrected by adding concentrated HCl or NaOH. Protein solutions (9 μM) were prepared by diluting a concentrated stock solution (200 μM) in the desired buffer. The concentration of protein was determined after each experiment by UV–visible spectroscopy using $\varepsilon_{401} = 188\,000\ M^{-1}\ cm^{-1}$ [11] for the oxidized protein. The reducing agent, sodium dithionite was prepared in the same buffer for the experiments at pH 7 and pH 8. For the experiments below pH 7, solutions were prepared in 5 mM sodium phosphate buffer pH 7 to avoid dithionite decomposition in acidic conditions, with NaCl added to the desired ionic strength. After each experiment the actual pH of the reaction was measured. Also, for each experiment the actual concentration of sodium dithionite was measured by UV–visible spectroscopy using $\varepsilon_{314} = 8\,000\ M^{-1}\ cm^{-1}$ [25] and the values were in the range 100–200 μM after mixing.

2.5. Analysis of kinetic data

Observed rate constants (k_{obs}) were obtained by single exponential fitting of the kinetic traces using the analysis tools provided by the stopped-flow software Kinetic Studio. The reported k_{obs} values are the average of at least three independent curves obtained at different wavelengths and different time scales and the errors were calculated from the standard deviations. The nature of the reducing agent was determined according to the method of Lambeth and Palmer [26]. Second-order rate constants k were obtained using Eq. (1):

$$k = k_{obs}(K_{diss} \times [\text{dithionite}])^{-1/2} \quad (1)$$

where K_{diss} is the equilibrium dissociation constant of sodium dithionite. The variation of K_{diss} with ionic strength was taken into account as described by Quintas and co-workers [24] (included as Supplementary Material).

Marcus theory applied to the Debye–Hückel formalism (Eq. (2)) [24,27] was used to fit the dependence of the second order rate constants on the ionic strength and obtain the effective charge on the protein surface (Z_1), which is relevant for the electrostatic interaction with the exogenous electron donor, hereafter designated by effective charge, and the value of the second order rate constant extrapolated to infinite ionic strength (k_∞)

$$1nk = 1nk_\infty - 3.576\left(\frac{\exp\left(-\kappa R_1\sqrt{I}\right)}{1+\kappa R_2\sqrt{I}} + \frac{\exp\left(-\kappa R_2\sqrt{I}\right)}{1+\kappa R_1\sqrt{I}}\right)\left(\frac{Z_1 Z_2}{R_1+R_2}\right). \quad (2)$$

In this equation $\kappa = 0.329\ Å^{-1}\ M^{-½}$ at 298 K, R_1 and R_2 are the radii, and Z_1 and Z_2 are the charges of the reactants. For the reducing agent $R_2 = 1.5$ Å [28] and $Z_2 = -1$ were used in the calculations. The effective radius of the protein was considered equal to the distance between the iron and the carboxylate group of the heme propionate, $R_1 = 8$ Å.

3. Results and discussion

3.1. Thermodynamic studies

The redox titrations of sensor domains GSU582 and GSU935 followed by visible spectroscopy in the physiological pH range for *Gs* growth at two ionic strengths (10 mM and 200 mM) are shown in Fig. 1. The previous spectroscopic characterization showed that the change in the redox state of the sensor domains is coupled to a heme spin state/coordination alteration [11,17]. This would imply conformational changes in the heme region, in particular at the distal ligand position. However, with exception of sensor GSU582 at pH 6, no hysteresis was observed, as the reductive and oxidative curves are superimposable, indicating that the redox process is fully reversible. Even for sensor GSU582, the hysteresis is not significant since the reductive and oxidative curves differ by less than 10 mV. The midpoint reduction potentials obtained from the fitting of the Nernst equation to each curve are indicated in Table 1. The reduction potential values are negative for both heme sensors but cover different working potential ranges (*cf.* Table 1 and Fig. 1). The negative values for the reduction potentials are well framed within the typical anoxic subsurface environments in which *Geobacter* species predominate [29–33] suggesting that the *c*-type heme group might work primarily as redox sensor in *G. sulfurreducens*' periplasm.

The reduction potential values of sensors GSU582 and GSU935 are affected by the ionic strength of the solution. For both proteins, the reduction potential increase with the ionic strength (*cf.* Table 1 and Fig. 2), an effect that is more noticeable for GSU935, particularly at high pH. As the ionic strength increases, the electrostatic effect of charged residues located in the vicinity of the heme groups is reduced by counter ion shielding effects. Thus, the observed increase of the reduction potential values suggests that the dominant charged residues in the vicinity of the heme groups are negative.

The midpoint reduction potential of both sensors is pH dependent (redox-Bohr effect) in the physiological range for *Gs* growth and those of GSU935 sensor are the ones most affected (Fig. 2). The decrease in the reduction potential values with pH leads to a progressive stabilization of the oxidized form, which can be explained on a purely electrostatic basis: the progressive deprotonation of an acid/base group in the vicinity of the heme groups is expected to lower its affinity for electrons with the concomitant decrease of the reduction potential values.

The variation in the reduction potential of a heme affected by a single proton is given by Eq. (3) [34], where the superscripts *red* and *ox* indicate the K_a values of the ionizable group with the heme reduced or oxidized and *basic* indicates the limiting value of E_m at high pH

$$E_m = E_0^{basic} - \frac{RT}{F}1n\left(\frac{1+\frac{[H^+]}{K_a^{ox}}}{1+\frac{[H^+]}{K_a^{red}}}\right). \quad (3)$$

The larger pH dependence of the reduction potential observed for GSU935 must reflect a stronger electron–proton interaction, which could be the result of a smaller distance between the heme and the ionizable group or a smaller dielectric constant of the intervening medium. However, it could also be caused by the involvement of a second ionizable group. The expression for two distinct and non-interacting protons labeled α and β is given in Eq. (4), which is the simple sum of the effects of the two protons

$$E_m = E_0^{basic} - \frac{RT}{F}1n\left(\frac{\left(1+\frac{[H^+]}{K_{a\alpha}^{ox}}\right)\left(1+\frac{[H^+]}{K_{a\beta}^{ox}}\right)}{\left(1+\frac{[H^+]}{K_{a\alpha}^{red}}\right)\left(1+\frac{[H^+]}{K_{a\beta}^{red}}\right)}\right). \quad (4)$$

The observable macroscopic values are related to these by Eq. (5):

$$K_{aA} = \frac{K_{a\alpha}K_{a\beta}}{K_{a\alpha}+K_{a\beta}}; K_{aB} = K_{a\alpha} + K_{a\beta} \quad (5)$$

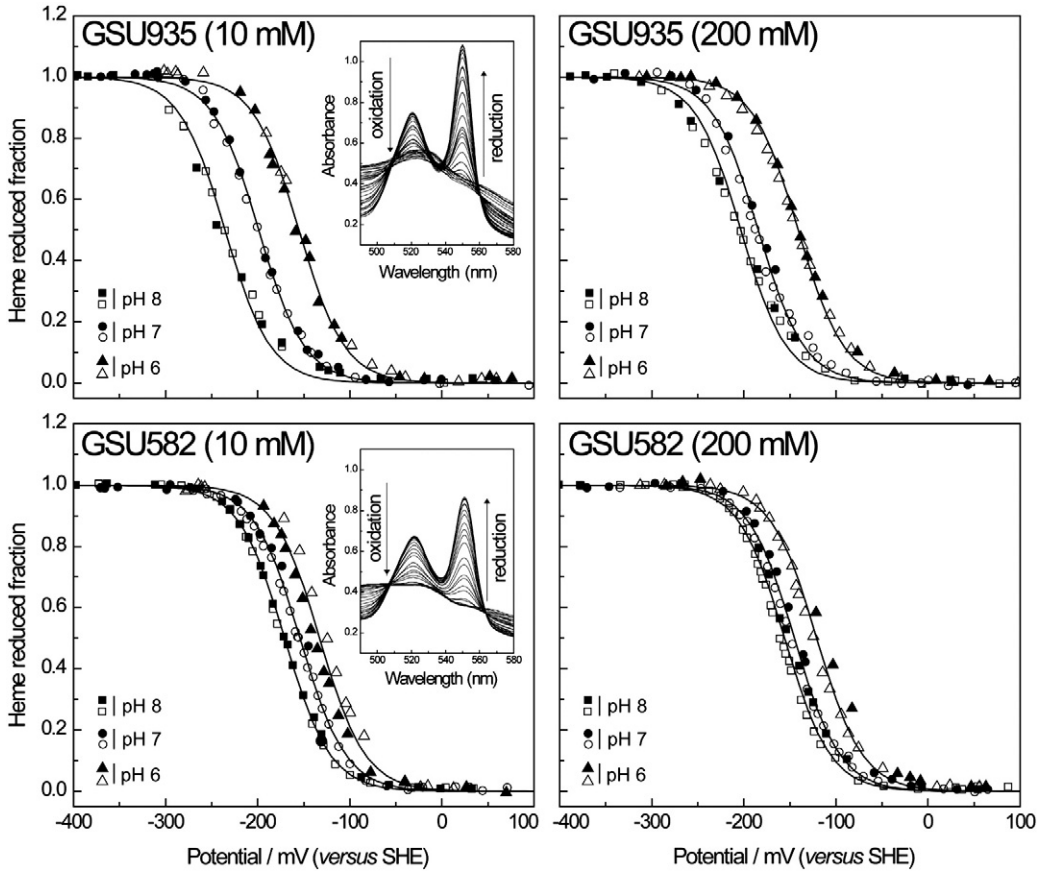

Fig. 1. Redox titrations followed by visible spectroscopy for GSU935 and GSU582 sensor domains at different pH and ionic strength values (10 mM and 200 mM). The triangles correspond to the curves obtained at pH 6, the circles at pH 7 and squares at pH 8. The open and filled symbols represent the data points in oxidative and reductive titrations, respectively. The lines are the results of the fit to the Nernst equation for one-electron reduction. The reduction potentials obtained, relative to standard hydrogen electrode (SHE), are listed in Table 1. As an example, the inset illustrates the α and β band regions of the visible spectra for sensors GSU935 and GSU582 at pH 7 acquired during the redox titration. The arrows in the insets indicate the direction of reduction and oxidation.

where A and B refer to the first and second acid/base equilibrium, respectively. The effect of two protons becomes indistinguishable from that of a single proton when the microscopic K_a values for the individual groups are $K_{a\alpha}^{ox} = K_a^{ox}$, $K_{a\beta}^{red} = K_a^{red}$ and $K_{a\alpha}^{red} = K_{a\beta}^{ox}$. It is therefore impossible to distinguish the effect of one or two protons from the slope of the pH dependence of the reduction potential. Additional information must be obtained from different experiments to be able to discriminate if the redox-Bohr effect involves one or two protons. In this work, information obtained from the analysis of kinetic and structural data was used to distinguish between the two, as discussed below.

3.2. Kinetic studies

To determine the nature of the reducing species, the rate of reduction of GSU582 and GSU935 was studied as a function of the concentration of sodium dithionite [28]. The linear dependence of the observed rate constants (k_{obs}) on the square root of the concentration of sodium dithionite (Fig. 3) showed that the reducing species is the bisulfite radical ($SO_2^{\bullet -}$) for both sensors. Despite the low value of the equilibrium dissociation constant of sodium dithionite, the concentration of $SO_2^{\bullet -}$ can be considered constant due to the very fast dissociation rate and the high concentration of sodium dithionite compared to the protein, making the reaction between $SO_2^{\bullet -}$ and the sensors pseudo-first-order. To obtain information on the nature and intensity of charges in the vicinity of the hemes, the GSU582 and GSU935 rate of reduction by sodium dithionite was studied as a function of ionic strength at different pH values using the stopped-flow technique. As an example the time course traces obtained for both sensors at pH 7 and 200 mM ionic strength are shown in Figure S2 (Supplementary Material). The

Table 1
Midpoint reduction potentials in mV (*versus* SHE) of heme sensor domains GSU582 and GSU935 measured at different pH and ionic strength values in mM.

pH	6		7		8	
Ionic strength	10	200	10	200	10	200
GSU582	−133	−121	−154	−145	−171	−156
GSU935	−155	−141	−199	−184	−235	−203

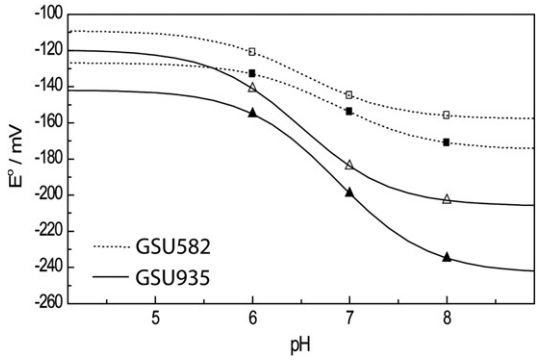

Fig. 2. pH dependence of the reduction potential (E_m) of sensors GSU582 (squares) and GSU935 (triangles). Data points are represented by symbols (solid symbols for 10 mM ionic strength and void symbols for 200 mM ionic strength). The lines were simulated with Eqs. (3) and (4) and are an illustration of the transfer of one electron coupled to one proton (dashed lines) or one electron coupled to two identical protons (solid lines). If a single proton (Eq. (3)) were used to simulate all the data, the difference $pK_a^{red} - pK_a^{ox}$ would be about 1 pH unit in GSU582 and about 2 pH units in GSU935.

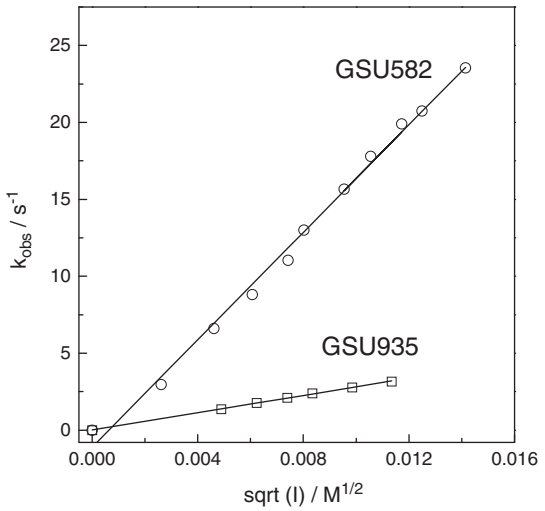

Fig. 3. Dependence of the observed rate constants (k_{obs}) on the square root of the sodium dithionite concentration at pH 7 (squares and circles correspond to GSU935 and GSU582, respectively). The dashed lines are the result of the linear fit to the data points.

second order rate constants calculated from the observed rate constants, as described in Section 2, are included in a Table in Supplementary Material. The logarithm of the second order rate constants as a function of the square root of the ionic strength, at different pH values, is presented in Fig. 4. From the positive slope of the curves it can be concluded that the electrostatic interaction between the redox partners is repulsive because the shielding of the charges at high ionic strength leads to an increase of the rate constant. Since the reducing species is negatively charged, the effective charge on the protein must be also negative for both sensors.

The rate constants of GSU582 are higher than those of GSU935, which might be a consequence of the larger driving force for the electron transfer reaction. The reducing species is $SO_2^{\bullet -}$ and the couple $SO_2/SO_2^{\bullet -}$ has a reduction potential −0.3 V, which is independent of pH above pH = 2 [35]. Since the reduction potential of GSU582 is less negative than that of GSU935 (Table 1), this shows that GSU582 has a larger driving force for electron transfer. The rate constants of GSU582 are also independent of pH whereas those of GSU935 are clearly pH dependent, the rates decreasing with increasing pH. Because the slope increases with the intensity of the charge, the fact that the GSU935 curves

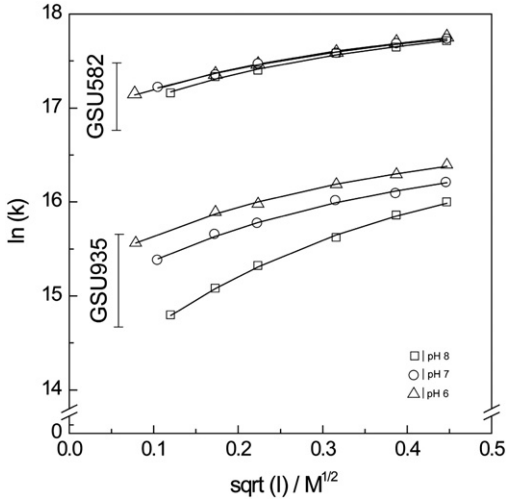

Fig. 4. Dependence of the logarithm of the second order rate constant for the reduction of the heme sensor domains by sodium dithionite, ln(k), on the square root of the ionic strength at different pH values for sensors GSU582 and GSU935 (triangles pH 6, circles pH 7 and squares pH 8). The lines are the result of the fit of Eq. (2) to the data points.

at pH 6 and pH 7 are nearly parallel shows that the charge does not change much in this pH range, thus the lower rate observed at pH 7 is probably due to a decrease in the driving force. However, the slope increases significantly going from pH 7 to pH 8, indicating that the effective charge on the protein becomes more negative. As expected, the repulsive effect of the extra negative charge is more apparent at low ionic strength.

A quantitative analysis based on Marcus theory applied to the Debye–Hückel formalism (Eq. (2)) makes it possible to obtain the effective charges of the two sensors at the different pH values and the rate constants extrapolated to infinite ionic strength. The results of the fit are presented in Table 2, together with the extrapolation of the reduction potentials of the heme sensor domains to infinite ionic strength, obtained as described by Quintas et al. [24], and included in Supplementary Materials.

The effective charge of GSU935 is slightly more negative than that of GSU582, suggesting the presence of a higher number of acidic groups in the region where $SO_2^{\bullet -}$ approaches the heme. The larger negative charge also contributes to the smaller rate constants measured for GSU935 at typical ionic strengths, but should not contribute to the difference between the rate constants of GSU935 and GSU582 at infinite ionic strength. The effective charge of GSU582 hardly changes in the pH range 6 to 8, whereas the charge of GSU935 changes by at least one unit between pH 7 and pH 8. These results indicate that in GSU935 there is at least one ionizable group that deprotonates in this pH range that is not present in GSU582. This group affects the electrostatic interaction between $SO_2^{\bullet -}$ and the protein and may also affect the reduction potential of the heme, depending on its location.

The effect of the driving force can be separated from the effect of the electrostatic interactions by comparing the ratios of rate constants at infinite ionic strength, obtained from the fit, with ratios of rate constants calculated for a given driving force, using Marcus theory for electron transfer [36] (Eq. (6)) [24]

$$\frac{k_{ET}^{pHi}}{k_{ET}^{pHj}} = \exp\left(\frac{\left(E_{GSU}^{pHi} - E_{GSU}^{pHj}\right)F}{2RT}\left(1 + \frac{E_{SO2}F}{\lambda} - \frac{\left(E_{GSU}^{pHi} - E_{GSU}^{pHj}\right)F}{2\lambda}\right)\right). \quad (6)$$

In Eq. (6) the E_{GSU} are the reduction potentials of the heme sensor domains at different pH values extrapolated to infinite ionic strength (see Table 2). A value of λ = 0.7 eV was used for the reorganization energy [37] and $E_{SO2} = -0.3$ V. For each sensor, the small variation in reduction potentials extrapolated to infinite ionic strength correlates well with the small variation in rates also extrapolated to infinite ionic strength (Table 3). However, comparison of the two sensors (Table 4) shows that the ratio of their rate constants extrapolated to infinite ionic strength cannot be explained solely on the basis of the difference in driving force. Since the difference in charge should have no effect at infinite ionic strength, it can be concluded that there are other structural factors that favor the interaction of $SO_2^{\bullet -}$ with GSU582 when compared to GSU935.

Table 2
Effective charge on the protein (Z_1), second order rate constant extrapolated to infinite ionic strength (k_∞) and reduction potential E_m^∞ extrapolated to infinite ionic strength, at different pH values for the heme sensor domains GSU582 and GSU935. The values of Z_1 and k_∞ were obtained with Eq. (2), as described in Section 2. The reduction potentials extrapolated to infinite ionic strength were obtained as described in the Supplementary Material.

	GSU582			GSU935		
	pH 6	pH 7	pH 8	pH 6	pH 7	pH 8
Z_1	−1.5	−1.4	−1.7	−2.1	−2.3	−3.8
$k_\infty/10^7 M^{-1} s^{-1}$	6.8	6.7	6.4	2.0	1.8	2.0
E_m^∞/mV	−129	−138	−144	−151	−173	−178

Table 3
Comparison between measured and predicted rate constants for each sensor domain. Ratios of the rate constants at different pH values (given as subscripts), extrapolated to infinite ionic strength, for each sensor (labeled as experimental) are compared with the expected ratios calculated using Marcus theory for electron transfer (Eq. (6) with reduction potentials extrapolated to infinite ionic strength).

	GSU582		GSU935	
	Experimental	Marcus	Experimental	Marcus
k_7/k_6	1.0	0.9	0.9	0.7
k_8/k_7	1.0	0.9	1.1	0.9

3.3. Structural correlations

The thermodynamic and kinetic studies for sensors GSU582 and GSU935 indicated that: (i) the dominant charged residues in the vicinity of the hemes are negative; (ii) the effective charge of GSU935 is more negative than that of GSU582; (iii) in GSU935 there is at least one ionizable group with a pK_a between 7 and 8 that is not present in GSU582, and (iv) the midpoint reduction potentials of both sensors decrease with increasing pH, with GSU935 sensor most affected. In order to rationalize these inferences we then moved to a detailed structural analysis of both sensors, in particular of their heme environment, noting that the charged groups which affect the interaction with $SO_2^{\bullet -}$ are not necessarily the same as those which affect the reduction potential. The crystal structures of GSU582 and GSU935 sensors were determined and showed that they form swapped-dimers with a PAS-type fold formed by polypeptide segments of the two monomers [17]. Also, each heme has axial ligands provided by both monomers. In solution, under the experimental conditions used in this work, the monomer–dimer equilibrium is shifted towards the monomeric form as previously described [18]. Models of GSU582 and GSU935 monomers in solution were previously constructed from the respective crystal structures [17] and were used in this work to rationalize the thermodynamic and kinetic observations.

The comparison between the structures of the swapped-dimers and monomers is depicted in Fig. 5. Despite the fact that some amino acid residues belong to a different polypeptide chain in the swapped dimer, the heme environment is expected to be similar in the monomers of both proteins (Fig. 5). Although the two heme sensor domains have similar structural folds, their distinct primary sequences (see Figure S1 in Supplementary Material) results in different distributions of electrostatic potential at the surfaces (Fig. 6A and B). However, both sensors show a predominantly negative electrostatic surface in the region of the heme groups (see Fig. 6), which explains the observed increase in the reduction potentials with the ionic strength for both sensors. A detailed comparison of the negative charges in the vicinity of the heme groups shows that in GSU935 there is a glutamic acid (E89) (accessible surface area of the E89 side chain is 59 Å^2), which has no counterpart in GSU582, with the equivalent residue being an Ala. An aspartic acid (D57) in GSU935 is within van der Waals contact distance pointing towards the heme and is fairly buried (accessible surface area of the D57 side chain is 7 Å^2), whereas the equivalent residue is Gly in GSU582. There is a glutamic acid residue present in GSU582 at position 58 (E58) fully exposed to the solvent (accessible surface area of the E58 side chain is 68 Å^2), which is farther from the heme with its side chain pointing away from the heme (*cf.* Fig. 6C and D). The heme propionates of the two sensor domains also show some structural differences: in GSU582 both heme propionates are fairly exposed to the solvent (surface exposure of propionates A and D are 49.6 Å^2 and 92.2 Å^2, respectively), whereas in GSU935 heme propionate A is rather buried when compared to heme propionate D (surface exposure of propionates A and D are 18.6 Å^2 and 77.9 Å^2, respectively). Therefore, sensor GSU935 has a more negative electrostatic surface around the heme group, which agrees with the lower reduction potentials and their higher ionic strength dependence, which is more noticeable at pH 8 as shown in Fig. 2.

The positive slope of the kinetic data in Fig. 4 was also indicative of a negative surface potential around the heme in both sensors. The effective charges calculated from these data (shown in Table 2) are also consistent with the more negative environment of the heme in GSU935 (see panels A and B of Fig. 6). The kinetic data also suggests the existence of an ionizable group with a pK_a value in the pH range 7–8 in GSU935 that is not present in GSU582. This group could also be responsible for the stronger redox-Bohr effect observed in GSU935. However, the pK_a observed in the rate constant is macroscopic (*cf.* Eq. (5)) and not necessarily the property of a single ionizable group. This pK_a will be shifted to a higher pH by the statistical effect and also by any interaction between the groups, and so the pK_a of the additional group in GSU935 may be below 7.

Given the structural differences described, it is also possible that different acid/base groups give major contributions either to the redox-Bohr effect or to the repulsive interaction with $SO_2^{\bullet -}$. It is likely that the two more buried carboxylic groups (D57 and propionate A) have a greater influence in the reduction potential of the heme, while the exposed E89 should play a bigger role in the electrostatic interaction with the electron donor.

Putting together thermodynamic, kinetic and structural information, it may be concluded that, although it is possible to simulate the pH dependence of the reduction potentials of the two sensors with a single acid/base group it is probable that an additional group plays a part in GSU935. Therefore, both sensors have at least one acid/base group that accounts for a difference between pK_{red} and pK_{ox} of about 1 pH unit and GSU935 has at least a second ionizable group that accounts for the rest of the redox-Bohr effect.

The comparison of the kinetic properties of the two sensors also showed that the difference in absolute rate constants measured cannot be fully explained by the difference in charge and driving force and there must be another structural factor involved. Since the reducing agent is a small inorganic ion, the solvent exposure of the heme may play a significant role [38]. The solvent exposure of the heme in the sensor domains was calculated with the program surface using default parameters within ccp4 package [39], and the values obtained were 234 Å for GSU582 and 180 Å for GSU935. The higher solvent exposure of the heme in sensor domain GSU582 could account for the fact that the reduction of GSU582 is nearly twice as fast as GSU935, when charge effects and driving force are discounted (see Table 4).

Table 4
Comparison of the rate constants of the two sensor domains. The ratios of the rate constants of the two sensors, extrapolated to infinite ionic strength at each pH value (labeled as experimental) are compared with the expected ratios determined using Marcus theory for electron transfer. Eq. (6) was used with the two sensors in place of two pH values and with reduction potentials extrapolated to infinite ionic strength.

k^{GSU582}/k^{GSU935} Infinite ionic strength		
pH	Experimental	Marcus
6	3.4	1.4
7	3.7	1.7
8	3.2	1.7

4. Conclusions

The detailed thermodynamic and kinetic characterization of periplasmic sensor domains of the methyl-accepting chemotaxis proteins GSU582 and GSU935 from *G. sulfurreducens* provided for the first time a rationalization for the co-existence of two methyl-accepting chemotaxis proteins with remarkably similar spectroscopic features and structural folds. The results obtained in the *Gs* physiological pH range for

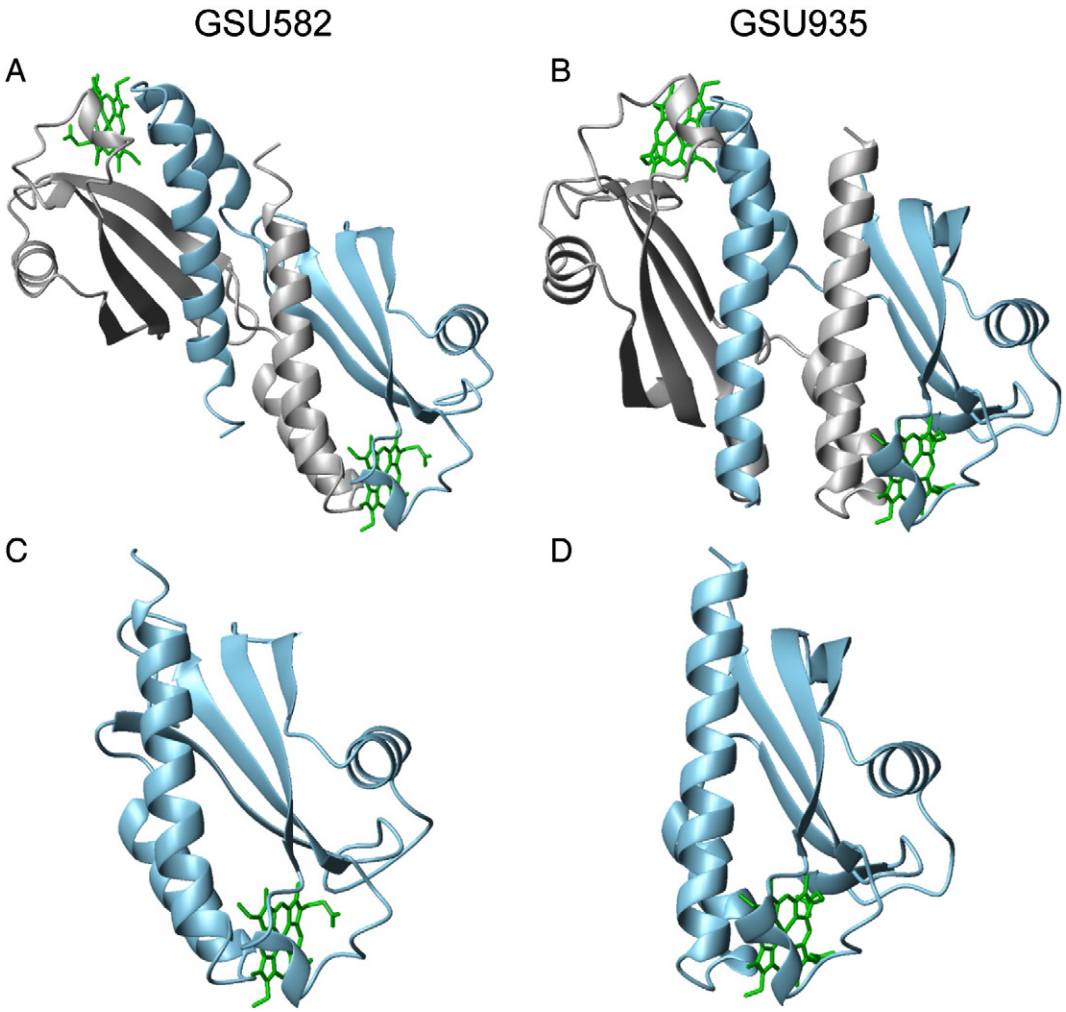

Fig. 5. Ribbon diagram of swapped dimers of heme sensors GSU582 (A) and GSU935 (B). The structures of sensors were retrieved from the Protein Data Bank (codes: 3B47 and 3B42). In the dimers the monomers are highlighted blue and gray and are presented in panels C and D, respectively. Figures were produced using MOLMOL [40].

growth showed that the properties of the sensor domains GSU935 and GSU582 are different. The thermodynamic studies showed that the sensor domain GSU935 displayed more negative reduction potentials, which are more strongly modulated by the pH (redox-Bohr effect) and ionic strength. Similarly, the kinetic studies showed that the rate constants of the sensor GSU935 are smaller, compared to those of GSU582, and are considerably more affected by the pH or ionic strength. The analysis of the structure of the two sensors allowed us to rationalize the thermodynamic and kinetic data and to understand the functional differences between the two sensors at molecular level: (i) the electrostatic surface in the heme neighborhoods is negative in both sensors, as determined from the kinetic studies with a negatively charged reducing agent, since the rate constants increase with the ionic strength; (ii) the more negative electrostatic surface around the heme group of sensor GSU935 correlates with the more negative reduction potentials, smaller rate constants, and with the larger negative charge predicted from the kinetic studies; (iii) the solvent exposure of the GSU582 heme group is larger, compared to that of GSU935, and might contribute to the higher rate constants observed in the former protein; (iv) the greater effective negative charge around the heme group of GSU935 may contribute to the higher redox-Bohr effect observed in this sensor domain, and might be explained by the close proximity of aspartic acid (D57) and propionate A; and (v) the kinetic data of GSU935 predicts an increase in the negative charge between pH 7 and 8, which could be explained by the deprotonation of the side chain of glutamic acid (E89), an exposed residue in the middle of a highly negative surface potential, that has no counterpart in GSU582. Overall, the distinct functional properties described here for the two heme sensor domains from *G. sulfurreducens* correlate with the structural data available and provide an excellent example of how functional properties of structurally related proteins from the same microorganism could be modulated by key residues placed in strategic positions. Finally, the good correlation observed between the thermodynamic and kinetic analysis and the available structural data, demonstrates that the strategy presented here for the two methyl-accepting chemotaxis proteins GSU582 and GSU935 from *G. sulfurreducens*, and elsewhere for cytochrome *c″* from *Methylophylus methylotrophus* [24] where the electrostatic interaction with the electron donor is attractive, can be used to obtain information on the electrostatic environment of the heme groups in the absence of structural models. This information might be important to understand, or predict, protein–protein interactions that are fundamental to *in vivo* electron transfer.

Acknowledgments

We thank Dr. Marianne Schiffer for the helpful discussions. This work was supported by the following grants: PTDC/BBB-BEP/0753/2012 (to CAS), PEst-C/EQB/LA0006/2013 (to REQUIMTE Laboratório

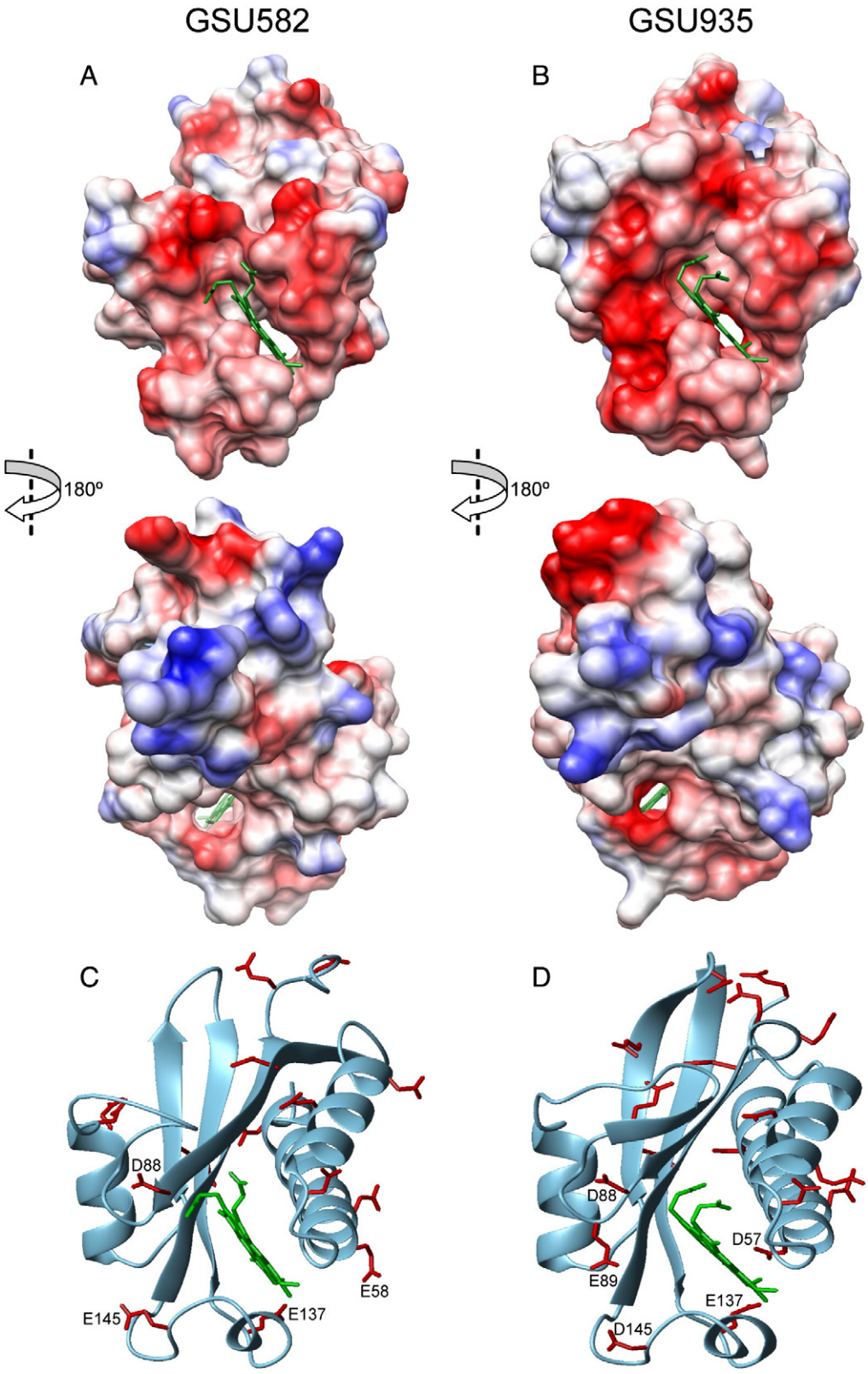

Fig. 6. Surface electrostatic potential around the heme region calculated by the program CHIMERA [41] for sensors GSU582 (A) and GSU935 (B). Red indicates negative and blue indicates positive potential. The heme groups are colored green. Ribbon diagram of GSU582 (C) and GSU935 (D) sensors. The peptide chain and the hemes are colored blue and green, respectively. The negatively charged residues are shown in red and those in the vicinity of the heme groups are labeled according to the amino acid sequence numbering. Figures were produced using MOLMOL [40].

Associado) and REEQ/336/BIO/2005 from Fundação para a Ciência e a Tecnologia (FCT), Portugal. MAS is the recipient of grant SFRH/BD/61952/2009 from FCT. PRP is partially supported by the division of Chemical Sciences, Geosciences, and Biosciences, Office of Basic Energy Sciences of the U.S. Department of Energy program under contract no. DE-AC02-06CH11357.

Appendix A. Supplementary data

Supplementary data to this article can be found online at http://dx.doi.org/10.1016/j.bbabio.2014.01.008.

References

[1] A.H. West, A.M. Stock, Histidine kinases and response regulator proteins in two-component signaling systems, Trends Biochem. Sci. 26 (2001) 369–376.
[2] A.M. Stock, V.L. Robinson, P.N. Goudreau, Two-component signal transduction, Ann. Rev. Biochem. 69 (2000) 183–215.
[3] G.H. Wadhams, J.P. Armitage, Making sense of it all: bacterial chemotaxis, Nat. Rev. Mol. Cell Biol. 5 (2004) 1024–1037.
[4] S. Aono, Biochemical and biophysical properties of the CO-sensing transcriptional activator CooA, Acc. Chem. Res. 36 (2003) 825–831.
[5] M.A. Gilles-Gonzalez, G. Gonzalez, Signal transduction by heme-containing PAS-domain proteins, J. Appl. Physiol. 96 (2004) 774–783.
[6] M.A. Gilles-Gonzalez, G. Gonzalez, Heme-based sensors: defining characteristics, recent developments, and regulatory hypotheses, J. Inorg. Biochem. 99 (2005) 1–22.
[7] G.P. Roberts, R.L. Kerby, H. Youn, M. Conrad, CooA, a paradigm for gas sensing regulatory proteins, J. Inorg. Biochem. 99 (2005) 280–292.
[8] E.M. Boon, M.A. Marletta, Ligand discrimination in soluble guanylate cyclase and the H-NOX family of heme sensor proteins, Curr. Opin. Chem. Biol. 9 (2005) 441–446.
[9] Y. Sasakura, T. Yoshimura-Suzuki, H. Kurokawa, T. Shimizu, Structure–function relationships of EcDOS, a heme-regulated phosphodiesterase from *Escherichia coli*, Acc. Chem. Res. 39 (2006) 37–43.
[10] S. Aono, Metal-containing sensor proteins sensing diatomic gas molecules, Dalton Trans. (2008) 3137–3146.
[11] T. Catarino, M. Pessanha, A.G. De Candia, Z. Gouveia, A.P. Fernandes, P.R. Pokkuluri, D. Murgida, M.A. Marti, S. Todorovic, C.A. Salgueiro, Probing the chemotaxis periplasmic sensor domains from *Geobacter sulfurreducens* by combined resonance Raman and molecular dynamic approaches: NO and CO sensing, J. Phys. Chem. B 114 (2010) 11251–11260.
[12] A. Farhana, V. Saini, A. Kumar, J.R. Lancaster Jr., A.J. Steyn, Environmental heme-based sensor proteins: implications for understanding bacterial pathogenesis, Antioxid. Redox Signal. 17 (2012) 1232–1245.
[13] D.R. Lovley, Environmental Microbe–Metal Interactions, ASM Press, Washington, D.C, 2000. 408.
[14] Y.Y. Londer, I.S. Dementieva, C.A. D'Ausilio, P.R. Pokkuluri, M. Schiffer, Characterization of a *c*-type heme-containing PAS sensor domain from *Geobacter sulfurreducens* representing a novel family of periplasmic sensors in Geobacteraceae and other bacteria, FEMS Microbiol. Lett. 258 (2006) 173–181.
[15] R. Fu, J.D. Wall, G. Voordouw, DcrA, a *c*-type heme-containing methyl-accepting protein from *Desulfovibrio vulgaris* Hildenborough, senses the oxygen concentration or redox potential of the environment, J. Bacteriol. 176 (1994) 344–350.
[16] S. Yoshioka, K. Kobayashi, H. Yoshimura, T. Uchida, T. Kitagawa, S. Aono, Biophysical properties of a *c*-type heme in chemotaxis signal transducer protein DcrA, Biochemistry 44 (2005) 15406–15413.
[17] P.R. Pokkuluri, M. Pessanha, Y.Y. Londer, S.J. Wood, N.E. Duke, R. Wilton, T. Catarino, C.A. Salgueiro, M. Schiffer, Structures and solution properties of two novel periplasmic sensor domains with *c*-type heme from chemotaxis proteins of *Geobacter sulfurreducens*: implications for signal transduction, J. Mol. Biol. 377 (2008) 1498–1517.
[18] M.A. Silva, T.G. Lucas, C.A. Salgueiro, C.M. Gomes, Protein folding modulates the swapped dimerization mechanism of methyl-accepting chemotaxis heme sensors, PLoS One 7 (2012) e46328.
[19] E. Arslan, H. Schulz, R. Zufferey, P. Kunzler, L. Thony-Meyer, Overproduction of the *Bradyrhizobium japonicum c*-type cytochrome subunits of the cbb3 oxidase in *Escherichia coli*, Biochem. Biophys. Res. Commun. 251 (1998) 744–747.
[20] C.A. Salgueiro, L. Morgado, B. Fonseca, P. Lamosa, T. Catarino, D.L. Turner, R.O. Louro, Binding of ligands originates small perturbations on the microscopic thermodynamic properties of a multicentre redox protein, FEBS J. 272 (2005) 2251–2260.
[21] R.O. Louro, T. Catarino, J. LeGall, D.L. Turner, A.V. Xavier, Cooperativity between electrons and protons in a monomeric cytochrome c(3): the importance of mechano-chemical coupling for energy transduction, ChemBioChem 2 (2001) 831–837.
[22] M. Pessanha, L. Morgado, R.O. Louro, Y.Y. Londer, P.R. Pokkuluri, M. Schiffer, C.A. Salgueiro, Thermodynamic characterization of triheme cytochrome PpcA from *Geobacter sulfurreducens*: evidence for a role played in e(−)/H+ energy transduction, Biochemistry 45 (2006) 13910–13917.
[23] M. Pessanha, Y.Y. Londer, W.C. Long, J. Erickson, P.R. Pokkuluri, M. Schiffer, C.A. Salgueiro, Redox characterization of *Geobacter sulfurreducens* cytochrome c(7): physiological relevance of the conserved residue F15 probed by site-specific mutagenesis, Biochemistry 43 (2004) 9909–9917.
[24] P.O. Quintas, A.P. Cepeda, N. Borges, T. Catarino, D.L. Turner, Relative importance of driving force and electrostatic interactions in the reduction of multihaem cytochromes by small molecules, Biochim. Biophys. Acta 1827 (2013) 745–750.
[25] M. Dixon, The acceptor specificity of flavins and flavoproteins. I. Techniques for anaerobic spectrophotometry, Biochim. Biophys. Acta 226 (1971) 241–258.
[26] D.O. Lambeth, G. Palmer, The kinetics and mechanism of reduction of electron transfer proteins and other compounds of biological interest by dithionite, J. Biol. Chem. 248 (1973) 6095–6103.
[27] S. Wherland, H.B. Gray, Metalloprotein electron transfer reactions: analysis of reactivity of horse heart cytochrome *c* with inorganic complexes, Proc. Natl. Acad. Sci. U. S. A. 73 (1976) 2950–2954.
[28] R.J. Balahura, M.D. Johnson, Outer-sphere dithionite reductions of metal complexes, Inorg. Chem. 26 (1987) 3860–3863.
[29] F. Caccavo Jr., D.J. Lonergan, D.R. Lovley, M. Davis, J.F. Stolz, M.J. McInerney, *Geobacter sulfurreducens* sp. nov., a hydrogen- and acetate-oxidizing dissimilatory metal-reducing microorganism, Appl. Environ. Microbiol. 60 (1994) 3752–3759.
[30] D.R. Lovley, Dissimilatory metal reduction, Annu. Rev. Microbiol. 47 (1993) 263–290.
[31] D.R. Lovley, D.E. Holmes, K.P. Nevin, Dissimilatory Fe(III) and Mn(IV) reduction, Adv. Microb. Physiol. 49 (2004) 219–286.
[32] D.R. Lovley, E.J.P. Phillips, Y.A. Gorby, E.R. Landa, Microbial reduction of uranium, Nature 350 (1991) 413–416.
[33] D.R. Lovley, M.J. Baedecker, D.J. Lonergan, I.M. Cozzarelli, E.J.P. Phillips, D.I. Siegel, Oxidation of aromatic contaminants coupled to microbial iron reduction, Nature 339 (1989) 297–300.
[34] P.L. Dutton, Redox potentiometry: determination of midpoint potentials of oxidation–reduction components of biological electron-transfer systems, Methods Enzymol. 54 (1978) 411–435.
[35] P. Neta, R.E. Huie, A. Harriman, One-electron-transfer reactions of the couple SO_2/SO_2^- in aqueous solutions. Pulse radiolytic and cyclic voltammetric studies, J. Phys. Chem. 91 (1987) 1606–1611.
[36] R.A. Marcus, N. Sutin, Electron transfers in chemistry and biology, Biochim. Biophys. Acta 811 (1985) 265–322.
[37] M. Sulpizi, S. Raugei, J. VandeVondele, P. Carloni, M. Sprik, Calculation of redox properties: understanding short- and long-range effects in rubredoxin, J. Phys. Chem. B 111 (2007) 3969–3976.
[38] C.M. Paquete, D.L. Turner, R.O. Louro, A.V. Xavier, T. Catarino, Thermodynamic and kinetic characterisation of individual haems in multicentre cytochromes c_3, Biochim. Biophys. Acta 1767 (2007) 1169–1179.
[39] B. Lee, F.M. Richards, The interpretation of protein structures: estimation of static accessibility, J. Mol. Biol. 55 (1971) 379–400.
[40] R. Koradi, M. Billeter, K. Wuthrich, MOLMOL: a program for display and analysis of macromolecular structures, J. Mol. Graph. 14 (1996) 51–55(29–32).
[41] E.F. Pettersen, T.D. Goddard, C.C. Huang, G.S. Couch, D.M. Greenblatt, E.C. Meng, T.E. Ferrin, UCSF Chimera—a visualization system for exploratory research and analysis, J. Comput. Chem. 25 (2004) 1605–1612.